1993

Synthesis, Superconductivity and ESR Characterization of Rb3C60 Crystals

J. A. Schlueter

U. Welp

H. H. Wang

U. Geiser

J. M. Williams

See next page for additional authors

Recommended Citation

Published in Physica C, Vol. 216: 305-314, 1993 http://www.sciencedirect.com/science/journal/09214534

Synthesis, superconductivity and ESR characterization of Rb_3C_{60} crystals

J.A. Schlueter, U. Welp, H.H. Wang [1], U. Geiser, J.M. Williams, M.J. Bauer, J.M. Cho, J.L. Smart and S.A. Taha

Chemistry and Materials Science Divisions, Argonne National Laboratory, Argonne, IL 60439, USA

A one-step doping process of C_{60} crystals with three equivalents of rubidium to produce Rb_3C_{60} crystals was developed. The T_c's for all Rb_3C_{60} crystalline samples ($\sim$30.5 K) were higher than those of the powder samples (28 to 29.6 K), but consistent with the reported four-probe resistivity result for a doped C_{60} crystal (transition midpoint = 30.2 K). High superconducting shielding fractions (between 60 and 90%) and sharp magnetic transition widths (ΔT_{10-90} between $\sim$3 K and 0.7 K) were observed for the samples doped with Rb at temperatures of 300 to 450°C. The doping process, as well as the composition, of these samples were studied with the use of an ESR spectrometer. Two major components, RbC_{60} and Rb_3C_{60}, were quantitatively characterized. The superconducting shielding fractions of these samples were found to be linearly correlated with the Rb_3C_{60} content obtained from ESR measurements. Higher-temperature doping (>400°C) favored the formation of Rb_3C_{60} at the expense of severe C_{60} crystal fragmentation. The optimal doping condition to produce Rb_3C_{60} crystals was found to be around 300°C.

1. Introduction

C_{60}, a new form of carbon allotrope, has attracted an intense amount of research interest [1]. The discovery of superconductivity in the potassium-doped C_{60} material has established a new molecular building block for three-dimensional superconductors [2]. A series of superconducting compounds with composition M_3C_{60} (M: alkali metal) have since been synthesized [3–8]. The highest T_c ($\sim$33 K) in this family was found for the composition $RbCs_2C_{60}$ [6]. In contrast to the one- or two-dimensional organic superconductors based on radical–cation salts [9], where superconductivity is often hampered by intervening charge-density-wave or spin-density-wave instabilities, packing of the spherical superatom C_{60} leads to a simple face centered cubic (fcc) lattice [10,11], where superconductivity effectively competes with other instabilities. Much research has focused on the orientational degrees of freedom of the C_{60} molecule [12,13], as well as the importance of electron correlation [14,15], and inter- and intramolecular vibration modes for the occurrence of superconductivity in alkali-doped samples [16–18].

Polycrystalline or powder samples most commonly used in physical measurements, are usually prepared in a two-step process. Initially, C_{60} powders are mixed with a stoichiometric amount of alkali metal and heated for several days (mixing stage) [3,4]. The doped samples are then pelletized and sintered at a higher temperature for several additional days (annealing stage), which results in superconducting shielding fractions approaching 100% (without demagnetization correction [5]). For salts produced in this manner, the superconducting transition widths (10 to 90% transition, ΔT_{10-90}) are greater than 10 K. In order to improve the sample quality and to sharpen the superconducting transition widths, single crystals Of C_{60} have been doped [14,15,19]. Sharp resistive transitions with a transition width $\sim$200 mK have been reported [14], but bulk superconductivity cannot be demonstrated in a resistivity experiment. In this paper we describe a one-step process allowing for the production of

[1] Author to whom correspondence should be addressed.

Rb_3C_{60} crystals which show sharp inductive superconducting transitions ($\Delta T_{10-90} \sim 0.7$ K) and shielding fractions larger than 90% (without demagnetization correction).

2. Experimental

2.1. Starting materials

C_{60} was extracted from graphite soot (Strem Chemicals, Inc.) with toluene and separated from higher fullerenes by use of flash chromatography on a Norit A/silica gel column with toluene as the eluant [20]. Rubidium (99+%, courtesy of J.E. Schirber, Sandia National Laboratories) was used without further purification. Quartz reaction tubes were assembled in an argon-filled dry box and the manipulation carried out on a vacuum/argon manifold due to the highly flammable nature of elemental rubidium and rubidium-doped C_{60} salts.

2.2. Preparation of C_{60} crystals

Crystals Of C_{60} were prepared by vacuum sublimation [21] or vapor transport methods [22]. In our hands, the former procedure gave typical yields of ~40% and average C_{60} crystal size of ~0.5 mm. The latter procedure was more convenient and efficient. The average yield, based on three runs, was 70%, and a typical crystal size was ~1 mm. In a typical run, about 100 mg of C_{60} powder was loaded in a gold boat that was placed inside a quartz tube located in a three-zone furnace. High-purity He carrier gas was purged for half an hour. The three zones were then set to 600, 560 and 520°C, with the gold boat located near the center of the 600°C region. He gas was introduced from the 600°C end and swept through the three-zone furnace during the sublimation process. Well-formed C_{60} crystals (up to 3 mm) were harvested after 5 days in the 520°C zone.

2.3. Preparation of Rb_3C_{60} crystals

Approximately 10 mg of C_{60} crystals were accurately weighed and loaded into a 3 mm quartz tube. This tube was transfered into an argon-filled dry box and loaded with three equivalents of rubidium metal. The tube was sealed with a Cajon fitting, removed from the dry box, evacuated to 10^{-2} Torr on a Schlenk line, and flame sealed. This sealed glass tube was then heated in a furnace. After a designated period of time (see table 1), the sample was removed from the furnace and inspected visually. Typically, visual defects and crumbling of the doped crystals were observed. Any further manipulation of these air sensitive crystals was done under an argon atmosphere.

2.4. SQUID measurements

The magnetization of the samples was measured in a SQUID magnetometer (Quantum Design). T_c and the transition width were determined by cooling the sample in zero field (the magnet of the magnetometer was previously de-gaussed), then by applying a field of 1 G at 5 K and taking data while warming the sample up through the transition. The superconducting fraction was determined from the initial slope of the low-field magnetization curve at 5 K.

2.5. X-Ray measurements

Crystals to be examined by X-ray diffraction were individually sealed in thin-walled glass capillaries and mounted on an automated Nicolet P3/f four-circle diffractometer equipped with a molybdenum-sealed tube and a graphite monochromator ($\lambda = 0.7107$ Å). All X-ray diffraction experiments were carried out at room temperature. A poloroid type 57 film was employed for diffraction photographs on the diffractometer.

2.6. ESR measurements

An IBM ER-200 ESR spectrometer (X-band, 9.4 GHz) with a TE_{102} rectangular cavity was used. Low-temperature measurements were made with the use of an Oxford Instruments liquid-helium cryostat. A strong-pitch standard ($g = 2.0028$) was used for instrument calibration. A locally developed computer program was used to fit first derivative ESR spectra to a linear superposition of lorentzian derivatives [23]. Due to the cubic symmetry of the ESR active

species, no corrections for g-value anisotropy were applied.

3. Results and discussion

3.1. Synthesis and superconductivity

Superconducting transitions (samples B and G, table 1) with zero-field cooled data from the SQUID magnetometer are shown in fig. 1. In order to account for the different shielding fractions (see below), the susceptibility was normalized to its value at 5 K. The absolute values of the volume susceptibility at 5 K for samples B and G were -1.7×10^{-2} and -7.2×10^{-2}, respectively (dimensionless CGS units, i.e., for perfect diamagnetism $\chi=-1/4\pi$). The magnetic onset temperature (T_c) for both samples was 30.5 ± 0.2 K.

The T_c's for all Rb_3C_{60} crystalline samples were higher than those of the powder samples (reported T_c's between 28 to 29.6 K) [3,4,18,24], but consistent with the four-probe resistivity result for a doped C_{60} crystal (transition midpoint = 30.2 K) [14]. The ΔT_{10-90} widths defined as the transition width between 10% and 90% of the saturated diamagnetic moment, are also indicated in table 1. For sample G, we observed a very sharp transition with $\Delta T_{10-90}\sim0.7$ K (see fig. 1). The shielding fraction (%) measured at 5 K is calculated from the slope of a plot of the diamagnetic moment versus magnetic field, as shown in fig. 2 (samples B and G).

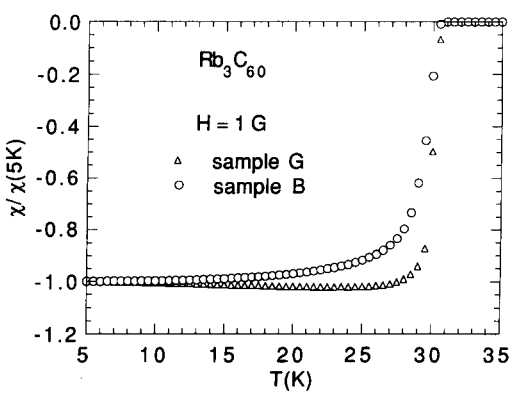

Fig. 1. The superconducting transition curves of Rb_3C_{60} crystals (Samples B and G) showing the magnetic onset temperatures and the transition widths. The magnetic moments of both samples are normalized to their 5 K values.

As indicated in table 1, sample A was doped at the relatively low temperature of 200°C for seven days. The resulting 12% shielding fraction indicated incomplete formation of Rb_3C_{60}. The transition width of 4.4 K, however, was greatly improved compared with that of the powder samples. A longer heating time at 200°C (sample B) further improved the shielding fraction. Sample C was heat-treated at 300°C for seven days resulting in a sharper transition width and a higher shielding fraction. Sample D was heat-treated at 400°C for only one day, and the superconducting shielding fraction reached 28%. Sample D was then split into two parts, D-1 and D-2, which were further treated at 400 and 450°C for 6 days, respectively. The superconducting shielding fraction reached 60 to 80%. Duplicate runs under the same conditions (samples E and F) reproduced the 60 to 80% shielding fraction range. For samples doped at 400 and 450°C, exfoliation of the crystals was quite noticeable due to the facile diffusion of alkali metal parallel to the [111] plane [25]. In order to determine if the samples were homogeneously doped, large crystallites were manually selected from small pieces to give sample F-1. The shielding fraction of F-1 (large crystals, 61%) is slightly lower but still comparable to that of the original sample F (77%). The result supported the idea that under the aforementioned experimental conditions, the doping process gave a nearly homogeneous sample.

Due to the exfoliation of C_{60} crystals during the higher-temperature doping process, a few large crystals (>1 mm) were selected to be doped at 300°C (sample G). After 6 days of doping, some exfoliation on the crystal surface was still noticeable but most crystals remained intact. The sample quality was very good considering its sharp transition width ($\sim$0.7 K) and high (90%) superconducting shielding fraction. A parallel experiment (sample H) was prepared from powdered C_{60} crystals and doped under the same conditions. The transition width was much broader (4.8 K) and the shielding fraction was quite low (4%). This result is consistent with a powder sample doped without compaction and annealing. The grain size of a typical powder sample is on the order of 1 μm [26], and the reported penetration depths for Rb_3C_{60} and K_3C_{60} are approximately

Table 1
SQUID measurements of the Rb_3C_{60} crystals [a),b)]

Rb_3C_{60} Sample [a),b)]	Mass (mg)	Experimental condition	ΔT_{10-90} (K)	Shielding fraction (%) [c)]
A	32.3	200°C, 7 days	4.4	12.0
B	7.1	200°C, 14 days	4.3	22.0
C	24.9	300°C, 7 days	3.0	23.5
D	20.4	400°C, 1 day	2.5	28.4
D-1 [d)]	5.8	400°C, 6 days [d)]	3.4	77.9
D-2 [d)]	8.6	450°C, 6 days [d)]	3.7	61.2
E	14.2	400°C, 6 days	1.8	65.1
F	14.2	450°C, 6 days	2.5	77.3
F-1 [e)]	7.0	- [e)]	2.6	61.0
G	13.8	300°C, 6 days	0.7	90.6
H	23.5	300°C, 6 days	4.8	4.0

[a)] Samples A through F were prepared from smaller C_{60} crystals with sizes ranging from 0.2 to 1.0 mm. Sample G was prepared from a few large (> 1 mm) C_{60} crystals and sample H was from smashed C_{60} crystals.
[b)] The mean-field superconducting transition temperature (T_{cl}) was 30.5 K for all samples except D-1 (30.0 K) and D-2 (29.5 K).
[c)] Superconducting shielding fraction measured at 5 K without demagnetization correction.
[d)] Samples D-1 and D-2 were resealed from sample D and subjected to additional heat treatment as indicated.
[e)] Sample F-1 contained the large crystallites manually separated from sample F without additional heat treatment.

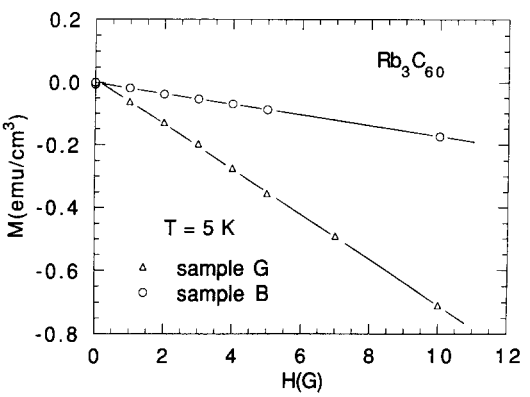

Fig. 2. A plot of magnetic moment vs. field of Rb_3C_{60} crystals (Samples B and G). The shielding fraction is calculated as $4\pi \times$ slope.

2400–4800 Å (0.24–0.48 μm) [27–29]. Low values of the superconducting shielding fraction are expected for powder samples unless the grain size is much larger than the penetration depth. The high shielding fraction and sharp transition in sample G (large C_{60} crystals doped at 300°C) was likely due to the much larger grain size.

3.2. X-ray diffraction

Individual crystals from batches D and F were examined by the use of single crystal diffraction. The sharp diffraction pattern of sample D could be indexed as a superposition of two face-centered cubic lattices with $a_1 = 14.14(1)$ Å and $a_2 = 14.13(1)$ Å, respectively, related by a 60° rotation around one of the body diagonals of the unit cell. The sharp diffraction pattern is due to unreacted C_{60}. Weak, diffuse scattered intensity, presumably from polycrystalline RbC_{60} and Rb_3C_{60}, was observed on a rotation photograph [30,31]. In sample F, the sharp diffraction pattern gave way to broad diffuse maxima superimposed upon noticeable complete powder rings. The maxima were too broad (5–10° in ω) to be centered automatically, but in the manual mode, the approximate angle settings of nine maxima could be obtained. They were indexable with a face-centered cubic cell with $a = 14.24(4)$ Å. Axial oscillation photographs revealed further maxima belonging to domains with different orientations. The visual examination of a rotation photograph yielded diffraction intensities indicative of the doped phases Rb_3C_{60} [30] and RbC_{60} [31], and very little, if any, unreacted C_{60}.

3.3. ESR characterization

A common impurity in the preparation of Rb_3C_{60} powder samples has previously been identified as RbC_{60} [32]. The 1:1 phase, RbC_{60}, when in a powder form, gave a sharp ESR signal with a peak-to-peak line width of ~6 G at room temperature [32]. The g-value for the RbC_{60} phase was 2.0007 ± 0.0011. The superconducting phase, Rb_3C_{60}, in powder form has a broader ESR line width around 12–14 G [32]. The g-value for the Rb_3C_{60} phase was practically the same as that of the RbC_{60} phase. Due to the broad solid-state spectra, there is a large uncertainty associated with the g-values, which prohibits meaningful comparison among the g-values of RbC_{60} and Rb_3C_{60}. For a mixture containing both RbC_{60} and Rb_3C_{60} phases, the ESR absorption of the individual overlapping components can be obtained from a line shape deconvolution program. The integrated ESR absorption of any specific phase is correlated to its molar concentration according to the following equations;

$$A_{RbC_{60}} = \chi_{RbC_{60}} \times [RbC_{60}]$$

$$= \chi_{RbC_{60}} \times \frac{\text{Wt. of } RbC_{60}}{\text{FW of } RbC_{60}}$$

and

$$A_{Rb_3C_{60}} = \chi_{Rb_3C_{60}} \times [Rb_3C_{60}]$$

$$= \chi_{Rb_3C_{60}} \times \frac{\text{Wt. of } Rb_3C_{60}}{\text{FW of } Rb_3C_{60}},$$

where A is the integrated absorption, χ is the ESR spin susceptibility, $[RbC_{60}]$ is the concentration of RbC_{60} in mole, Wt. is the weight in g, and FW is the formula weight in g/mole. The molar concentration of each phase can be obtained if the spin susceptibility χ is known. χ for RbC_{60} and Rb_3C_{60} can be estimated as follows:

$$\text{Total sample Wt.} = \text{Wt. of } RbC_{60} + \text{Wt. of } Rb_3C_{60}$$

$$= A_{RbC_{60}} \frac{\text{FW of } RbC_{60}}{\chi_{RbC_{60}}} + A_{Rb_3C_{60}} \frac{\text{FW of } Rb_3C_{60}}{\chi_{Rb_3C_{60}}}.$$

With two samples and two equations, $\chi_{RbC_{60}}$ and $\chi_{Rb_3C_{60}}$ can be obtained. The ratio $\chi_{Rb_3C_{60}}/\chi_{RbC_{60}}$ was thus determined to be 1.62, which is used to calculate the molar ratio of Rb_3C_{60}/RbC_{60} in all samples.

The rubidium-doping process of sample A (table 1) was monitored with the use of an ESR spectrometer. The sample was heated at 200°C and monitored after brief cooling to room temperature with ESR approximately every 20 h. Two major components were identified, RbC_{60} ($\Delta H_{pp} \sim 6$ G) and Rb_3C_{60} (ΔH_{pp} 10.5–12 G). The formation of both phases as a function of heating time is shown in fig. 3.

At 200°C, the growth rate for RbC_{60} was much faster than that of the Rb_3C_{60}. The observation was consistent with the recent report that RbC_{60} at 200°C is a stable phase-pure fcc compound with octahedral site occupancy only [31]. After doping at 200°C for 7 days, the Rb_3C_{60} content reached 13%, which was consistent with the result from SQUID measurements (12% shielding fraction). Doping at 300°C (sample C) was also monitored by the use of an ESR spectrometer. The growth patterns at 300°C for the first four days are shown in fig. 4.

At 300°C the growth rate of RbC_{60} was still faster but the growth rate of Rb_3C_{60} was significantly increased. For longer doping time ($\geq$ days), the peak-to-peak line widths for both phases became sharper. The 1:1 and 3:1 phases gave rise to ~5.5 G and ~8 G line widths, respectively. As the difference between the two line widths became smaller and since the difference in g-values was always small, the line-shape parameters became highly correlated. The resulting ESR line-shape refinement became unstable and no reliable signal deconvolution could be obtained. After 7 days doping at 300°C, sample C yielded a superconducting shielding fraction of 23.5% which was consistent with a higher Rb_3C_{60} content. A detailed analysis was carried out on the low-temperature data (50 K, see below) in order to avoid the correlated refinement parameters.

Sample D, after heating at 400°C for 1 day gave a strong but narrow ESR line width (7.3 G). Line-shape deconvolution of the room-temperature spectrum did not give a stable refinement due to the narrow line width and the highly correlated parameters. Sample D was split into two samples (D-1 and D-2) after the SQUID measurement. Sample D-1 was heat

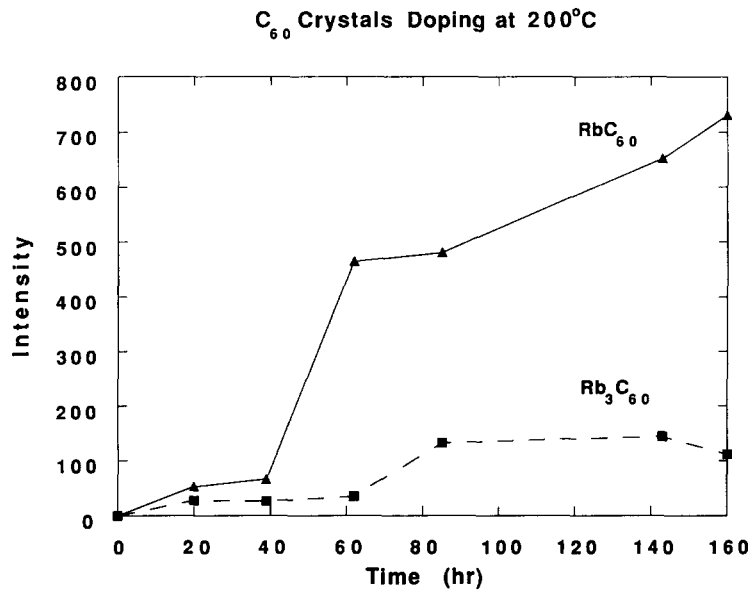

Fig. 3. The formation of the RbC_{60} and Rb_3C_{60} phases during the doping of C_{60} crystals with three equivalents of rubidium (Sample A) at 200°C.

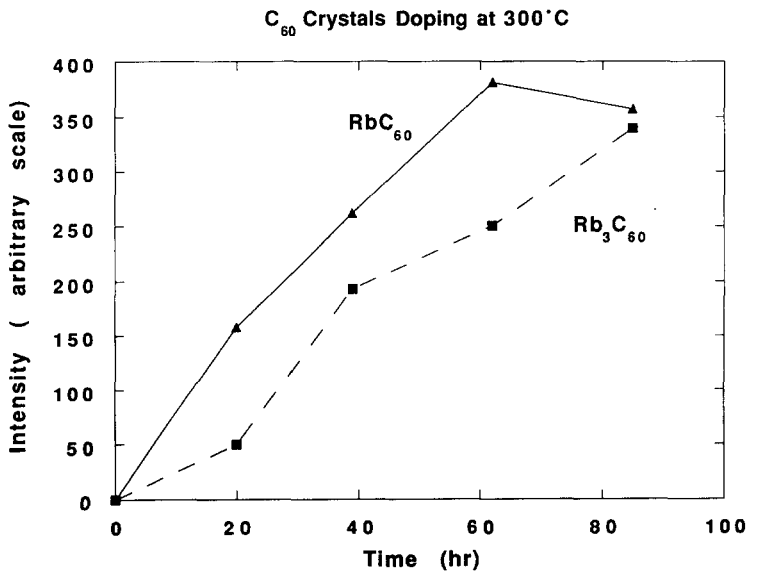

Fig. 4. The formation of the RbC_{60} and Rb_3C_{60} at 300°C (Sample C) for the first four days.

treated at 400°C for an additional six days. Since the room-temperature spectrum did not yield a satisfactory signal deconvolution, variable-temperature ESR measurements were carried out. The overall peak-to-peak line widths (triangles) and relative spin susceptibilities (squares) of sample D-1 were plotted

against temperature between 296 and 4 K in fig. 5.

As shown in fig. 5, the apparent overall line width decreased monotonically with decreasing temperature from 5.5 G at 296 K to 2.1 G at 70 K. In the same temperature range, the relative spin susceptibility was nearly a constant (fluctuating between 1.00 and 1.13), which was consistent with Pauli paramagnetism of a metallic specimen. Between 60 and 40 K, the spin susceptibility dropped by one order of magnitude while the peak-to-peak line width broadened from 2.4 G to ~4 G. Below 30 K, the ESR signal completely disappeared. At 30 K, a strong nonresonant magnetic hysteresis loop appeared during the forward and reverse ESR scans (fig. 6).

The disappearance of the resonant ESR signal and the appearance of the magnetic hysteresis loop is a clear signal of superconductivity in the sample. The appearance of a hysteresis loop in the modulated microwave absorption is caused by the screening supercurrents which are synchronous with the modulated field, and which shift the phase by 180° as the direction of the scan is reversed [33]. A narrow signal (~2.5 G) appeared below 9 K, which is likely due to the paramagnetic RbC_{60} impurity phase in an incompletely screened part of the sample.

We took advantage of the line-width broadening effect at 50 K and measured samples B through F-1 at that temperature. With the greater difference between RbC_{60} and Rb_3C_{60} line widths, the ESR line shape deconvolution procedure was very effective (see table 2).

As listed in table 2, at 50 K the RbC_{60} phase gave rise to a sharp ESR line width (ΔH_1) between 3.3 and 4.3 G, while the Rb_3C_{60} phase revealed a broader line width (ΔH_2) between 8 and 13 G. In order to check the validity of the phase assignment as well as the mole concentration, the mole percentage of Rb_3C_{60} content based on ESR analysis (table 2) was plotted against the superconducting shielding fraction obtained from SQUID measurements (table 1) in fig. 7.

The Rb_3C_{60} mole content in sample G was a rough estimate from the ESR analysis. Detailed line shape analysis awaits future study due to its strong Dysonian line shape. As shown in fig. 7, the superconducting shielding fraction was approximately proportional to the Rb_3C_{60} content calculated from ESR line shape analysis. This linear correlation unambig-

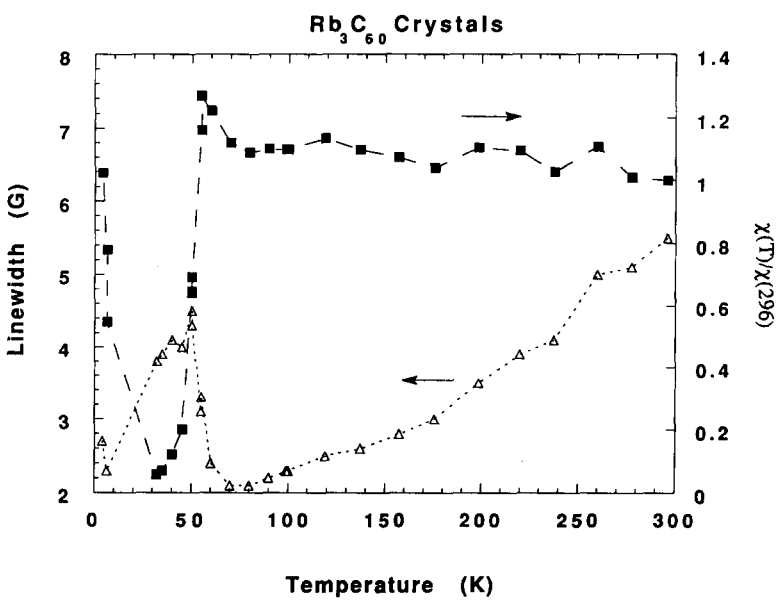

Fig. 5. The ESR peak-to-peak linewidth (triangles) and the relative spin susceptibility (squares) of Rb_3C_{60} (Sample D-1) plotted against temperature. The dashed lines are only used to guide the eyes. ESR signals from conduction electrons are not observed below 30 K due to the superconducting state.

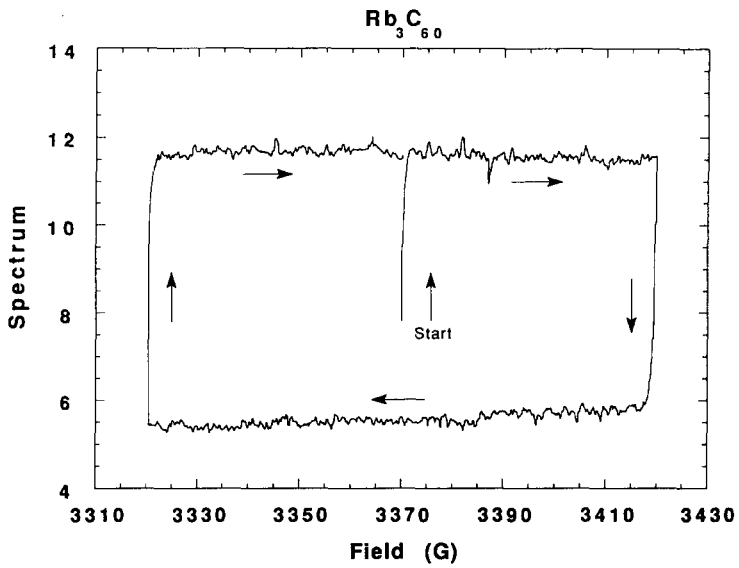

Fig. 6. The forward and reverse scans of sample D-1 at 20 K between 3320 G and 3420 G. Notice that the resonant ESR absorption near 3370 G has disappeared and the vertical offset of the forward and reverse scans is caused by the magnetic hysteresis of the superconducting sample and not by instrument settings.

Table 2
ESR analysis of the Rb_3C_{60} crystals [a]

Sample	RbC_{60}		Rb_3C_{60}		R [b] (%)
	ΔH_1 (G)	Mole %	ΔH_2 (G)	Mole %	
A	6.0	87	12.9	13	3.5
B	4.3	82	10.2	18	2.5
C	3.3	84	9.4	16	4.1
D-1	3.4	28	7.9	72	3.2
D-2	3.4	46	11.3	54	3.3
F	3.5	21	10.9	79	2.9
F-1	4.1	31	13.3	69	2.6

[a] The analyses were all based on low-temperature data (45 to 60 K) except sample A, which was based on room-temperature data.
[b] Agreement factor of fit: $R = 100\%\ (\Sigma|\text{obs}-\text{calc}|)/\Sigma|\text{obs}|$ for each spectrum; ca. 500 data points were used in the fit.

uously confirmed the Rb_3C_{60} phase assignment and the calculated mole percentage.

4. Conclusions

We have developed a one-step doping process to prepare crystals of Rb_3C_{60}. High superconducting shielding fractions (between 60% and 90%) can be obtained with a heat treatment between 300 and 450°C and no sample-pressing procedure is required during the process. Sharp magnetic transitions were observed in all Rb_3C_{60} crystalline samples due to their large grain sizes. The 1:1 RbC_{60} impurities were found in all Rb_3C_{60} samples. Doping large C_{60} crystals is a viable route to minimize the formation of the undesirable RbC_{60} phase. Higher temperature doping (>400°C) favored the formation of Rb_3C_{60} at the expense of severe C_{60} crystal fragmentation. The optimal doping condition for the formation of

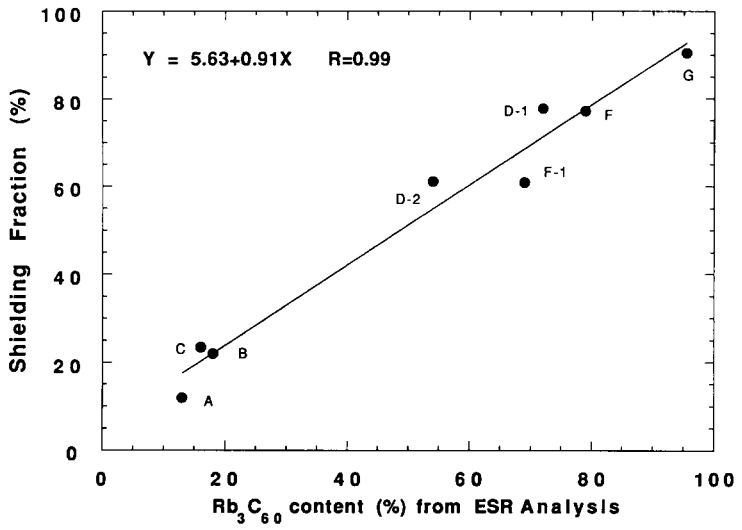

Fig. 7. A plot of the superconducting shielding fraction measured with a SQUID vs. Rb_3C_{60} molar content calculated from ESR analysis showing a linear correlation.

Rb_3C_{60} crystals was found to occur around 300°C. This simple one-step doping process provides high-quality crystals of Rb_3C_{60} for future study.

Acknowledgement

Work at Argonne National Laboratory is sponsored by the US Department of Energy (DOE), Office of Basic Energy Sciences, Division of Materials Sciences, under Contract W-31-109-ENG-38 and the NSF-Office of Science and Technology Center under contract STC-91-20000 (UW). MJB, JMC, JLS, and SAT are undergraduate student research participants sponsored by the Argonne Division of Educational Programs from the University of Wisconsin-Eau Claire, Eau Claire, WI; New Mexico State University, Las Cruces, NM; Western Montana College, Dillon, MT; and Stanford University, Stanford, CA, respectively.

References

[1] W. Krätschmer, L.D. Lamb, K. Fostiropoulos and D.R. Huffman, Nature (London) 347 (1990) 354.

[2] A.F. Hebard, M.J. Rosseinsky, R.C. Haddon, D.W. Murphy, S.H. Glarum, T.T.M. Palstra, A.P. Ramirez and A.R. Kortan, Nature (London) 350 (1991) 600.

[3] M.J. Rosseinsky, A.P. Ramirez, S.H. Glarum, D.W. Murphy, R.C. Haddon, A.F. Hebard, T.T.M. Palstra, A.R. Kortan, S.M. Zahurak and A.V. Makhija, Phys. Rev. Lett. 66 (1991) 2830.

[4] K. Holczer, O. Klein, S.-M. Huang, R.B. Kaner, K.-J. Fu, R.L. Whetten and F. Diederich, Science 252 (1991) 1154.

[5] C. Chen, S.P. Kelty and C.M. Lieber, Science 253 (1991) 886.

[6] K. Tanigaki, T.W. Ebbesen, S. Saito, J. Mizuki, J.S. Tsai, Y. Kubo and S. Kuroshima, Nature (London) 352 (1991) 222.

[7] M.J. Rosseinsky, D.W. Murphy, R.M. Fleming, R. Tycko, A.P. Ramirez, T. Siegrist, G. Dabbagh and S.E. Barrett, Nature (London) 356 (1992) 416.

[8] K. Tanigaki, I. Hirosawa, T.W. Ebbesen, J. Mizuki, Y. Shimakawa, Y. Kubo, J.S. Tsai and S. Kuroshima, Nature (London) 356 (1992) 419.

[9] J.M. Williams, J.R. Ferraro, R.J. Thorn, K.D. Carlson, U. Geiser, H.H. Wang, A.M. Kini and M.-H. Whangbo, Organic Superconductors (Including Fullerenes): Synthesis, Structure, Properties and Theory (Prentice Hall, New Jersey, 1992).

[10] P. Stephens, L. Mihaly, P.Lee, R.L. Whetten, S.-M. Huang, R.B. Kaner, F. Diederich and K. Holczer, Nature (London) 351 (1991) 632.

[11] O. Zhou, J.E. Fischer, N. Coustel, S. Kycia, Q. Zhu, A.R. McGhie, W.J. Romanow, J.P. McCauley Jr., A.B. Smith III and D.E. Cox, Nature (London) 351 (1991) 462.

[12] R.D. Johnson, C.S. Yannoni, H.C. Dorn, J.R. Salem and D.S. Bethune, Science 255 (1992) 1235.

[13] S.E. Barrett and R. Tycko, Phys. Rev. Lett. 69 (1992) 3754.
[14] X.-D. Xiang, J.G. Hou, G. Briceno, W.A. Vareka, R. Mostovoy, A. Zettl, V.H. Crespi and M.L. Cohen, Science 256 (1992) 1190.
[15] X.-D. Xiang, J.G. Hou, V.H. Crespi, A. Zettl and M.L. Cohen, Nature (London) 361 (1993) 54.
[16] T.W. Ebbesen, J.S. Tsai, K. Tanigaki, J. Tabuchi, Y. Shimakawa, Y. Kubo, I. Hirosawa and J. Mizuki, Nature (London) 355 (1992) 620.
[17] A.P. Ramirez, A.R. Kortan, M.J. Rosseinsky, S.J. Duclos, A.M. Musjce, R.C. Haddon, D.W. Murphy, A.V. Makhija, S.M. Zahurak and K.B. Lyons, Phys. Rev. Lett. 68 (1992) 1058.
[18] C.C. Chen and C.M. Lieber, Science 259 (1993) 655.
[19] H. Ogata, T. Inabe, H. Hoshi, Y. Maruyama, Y. Achiba, S. Suzuki, K. Kikuchi and I. Ikemoto, Jpn. J. Appl. Phys. 31 (1992) L166.
[20] W.A. Scrivens, P.V. Bedworth and J.M. Tour, J. Am. Chem. Soc. 114 (1992) 7917.
[21] R.L. Meng, D. Ramirez, X. Jiang, P.C. Chow, C. Diaz, K. Matsuishi, S.C. Moss, P.H. Hor and C.W. Chu, Appl. Phys. Lett. 59 (1991) 3402.
[22] J.Z. Liu, J.W. Dykes, M.D. Lan, P. Klavins, R.N. Shelton and M.M. Olmstead, Appl. Phys. Lett. 62 (1993) 531.
[23] L.K. Montgomery, U. Geiser, H.H. Wang, M.A. Beno, A.J. Schultz, A.M. Kini, K.D. Carlson, J.M. Williams, J.R. Whitworth, B.D. Gates, C.S. Cariss, C.M. Pipan, K.M. Donega, C. Wenz, K.W. Kwok and G.W. Crabtree, Synth. Met. 27 (1988) A195.
[24] H.H. Wang, A.M. Kini, B.M. Savall, K.D. Carlson, J.M. Williams, M.W. Lathrop, K.R. Lykke, D.H. Parker, P. Wurz, M.J. Pellin, D.M. Gruen, U. Welp, W.-K. Kwok, S. Fleshler, G.W. Crabtree, J.E. Schirber and D.L. Overmyer, Inorg. Chem. 30 (1991) 2962.
[25] P. Byszewski, R. Jablonski and S. Kolesnik, Solid State Commun. 84 (1992) 1111.
[26] D.W. Murphy, M.J. Rosseinsky, R.M. Fleming, R. Tycko, A.P. Ramirez, R.C. Haddon, T. Siegrist, G. Dabbagh, J.C. Tully and R.E. Walstedt, J. Phys. Chem. Solids 53 (1992) 1321.
[27] Y.J. Uemura, A. Keren, L.P. Le, G.M. Luke, B.J. Sternlieb, W.D. Wu, J.H. Brewer, R.L. Whetten, S.M. Huang, S. Lin, R.B. Kaner, F. Diederich, S. Donovan, G. Grüner and K. Holczer, Nature (London) 352 (1991) 605.
[28] K. Holczer, O. Klein, G. Grüner, J.D. Thompson, F. Diederich and R.L. Whetten, Phys. Rev. Lett. 67 (1991) 271.
[29] G. Sparn, J.D. Thompson, S. Huang, R.B. Kaner, F. Diederich, R.L. Whetten, G. Grüner and K. Holczer, Science 252 (1991) 1829.
[30] J.P. McCauley Jr., Q. Zhu, N. Coustel, O. Zhou, G.B.M. Vaughan, S.H.J. Idziak, J.E. Fischer, S.W. Tozer, D.M. Groski, N. Bykovetz, C.L. Lin, A.R. McGhie, B.H. Allen, W.J. Romanow, A.M. Demenstein and A.B. Smith III, J. Am. Chem. Soc. 113 (1991) 8537.
[31] Q. Zhu, O. Zhou, J.E. Fischer, A.R. McGhie, W.J. Romanow, R.M. Strongin, M.A. Cichy and A.B. Smith III, Phys. Rev. B, Rapid Commun. 47 (1993) 13948.
[32] J.A. Schlueter, H.H. Wang, M.W. Lathrop, U. Geiser, K.D. Carlson, J.D. Dudek, G.A. Yaconi and J.M. Williams, Chem. Mater. 5 (1993) 720.
[33] V.A. Atsarkin, V.V. Demidov and N.E. Noginova, Superconductivity 5 (1992) 301.